Symmetry breaking by quantum coherence in single electron attachment

E. Krishnakumar[1]*, Vaibhav S. Prabhudesai[1], Nigel J. Mason[2]

[1]Tata Institute of Fundamental Research, Homi Bhabha Road, Colaba, Mumbai 400005, India.

[2] Open University, Walton Hall, Milton Keynes, MK7 6AA, United Kingdom.

Coherently controlled interaction with photons is known to invoke quantum interference that removes the inversion symmetry in the dissociation of homonuclear diatomic molecules. But is it possible to observe this phenomenon in the interaction of incoherent electrons with such molecules? Here we show that resonant electron attachment to H_2 and its subsequent dissociation into H (n=2) + H^- is unexpectedly asymmetric about the inter-nuclear axis, while the asymmetry in D_2 is far less pronounced. We explain this counterintuitive observation as due to attachment of a single electron resulting in a coherent superposition two resonances of opposite parity. Apart from exemplifying a new process in studying quantum coherence phenomena, our observation of coherent quantum dynamics involving active participation of all three electrons and two nuclei should provide a new tool to study electron correlations which control all chemical processes and demonstrates the role of coherent effects in electron induced chemistry.

Quantum coherence induced effects in atomic and molecular processes are the foundations on which many concepts of quantum information technology are being developed [1]. These coherence properties are also the basis of several proposals for control of chemical reactions using lasers [2, 3]. The basic idea behind these control schemes has been to induce quantum coherence in molecular systems using coherent photon beams to establish more than one quantum path that may interfere with one another in order to achieve the desired outcome [4]. One of the most fascinating effects of such schemes is the breaking of inversion symmetry in a homonuclear diatomic molecule [5]. Since single photon absorption is dominated by dipole transitions, breaking the inversion symmetry present in any homonuclear diatomic system requires the simultaneous presence of two photon absorption paths. These coherent photon absorption paths, one of odd and the other of even parity interfere with one another such that the interference changes with the phase difference between the two photon paths. The crucial aspect in this process is the coherent transfer of odd and even angular momenta to a single molecule using two different sets of laser beams which are coherent with one another. Can such a phenomenon take place in particle collisions? In other words, will such quantum coherence be observed in a particle collision when more than one angular momentum transfer channels can be accessed with comparable strength to create a situation similar to the one and two photon interference process? If so, then such projectiles need not be coherent to invoke the quantum coherence in a

system. Here we show that this indeed happens in the case of electron attachment to hydrogen molecules.

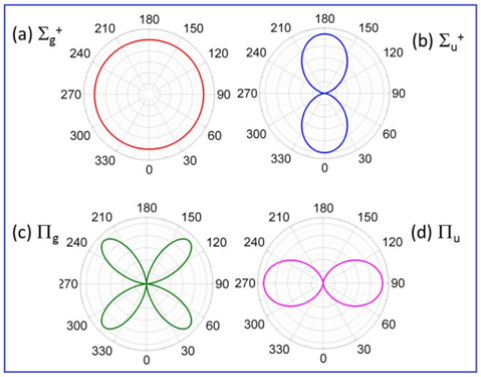

Fig. 1: Expected angular distribution with respect to the incoming electron beam (direction - from top to bottom) of the H^- ion formed in DA to H_2 in ground state Σ_g^+ in (a) Σ_g^+, (b) Σ_u^+, (c) Π_g and (d) Π_u states, with lowest allowed angular momentum transfer. These curves show the preferred orientations of the molecular axis for the electron capture for a given transition.

Electron attachment to a hydrogen molecule leading to the formation of an H^- ion and H atom in a process called dissociative attachment (DA) and together with its time reversed process where an H^- ion interacts with an H atom to form H_2 molecule and a free electron known as associative detachment (AD) is important in many areas of physics and chemistry from Cosmology [6-8] to the science and technology of controlled fusion [9, 10]. Resonant attachment is based upon the symmetry of the neutral state and the Negative Ion Resonance (NIR). It has been shown [11] that due to the inversion symmetry and subsequent parity conservation in homonuclear diatomic molecules like H_2, capture of only odd or even partial waves (angular momentum quanta) of the incoming electron is allowed. Indeed for a transition between states with same parity, capture of only even values of angular momentum quanta, l, are allowed and for opposite parity only odd values are allowed. Also, due to low energy of the projectiles, lower order partial waves tend to be more dominant compared to the higher order partial waves. Thus, in the case of H_2, where the molecule in the ground state has a Σ_g^+ symmetry, the formation of the NIR with Σ_g^+ symmetry allows all orientations of the molecule with respect to the incoming electron ($l = 0$ is the dominant partial wave) and the angular distribution of H^- will show little if any anisotropy as shown in Fig. 1a. Similarly, for the negative ion states Σ_u^+, Π_g and Π_u, the angular distributions are expected to be as shown in Fig.1b-d respectively. In any such case, the distribution is always symmetric with respect to the direction of the electron beam. DA experiments on all the homonuclear diatomic molecules studied to date, including H_2 (in the limited angular range) have consistently shown this symmetry [12-15].

H^- production from H_2 through DA appears as peaks in the cross section at 4 eV, 14 eV and as a broad peak between 7 and 13 eV [16]. The threshold for the formation of H^- from H_2 is 3.724 eV (bond dissociation energy of H_2 = 4.478 eV, electron affinity of H = 0.7545 eV). The 4 eV resonance dissociates to yield H^- ($1s^2$) + H (1s) with both fragments in their respective ground states. The broad peak between 7 eV and 13 eV is due to a purely repulsive NIR state which dissociates into the ground states of $H^-(1s^2)$ and H(1s). The 14 eV peak leads to $H^-(1s^2)$ and the excited H (n=2) atom (threshold 13.92 eV), hence the fragments are formed with very low kinetic energies similar to that of the 4 eV channel. H^- formation is also possible at higher electron energies, with opening of the new channel (dipolar dissociation) that has a threshold at 17.75 eV. It has been shown that between 14 eV and the dipolar dissociation threshold, DA leading to H^- and H (n=3, 4, etc.) does occur [17].

We carried out a series of experiments to measure the angular distribution of H^- produced by the DA to H_2 and D_2 using velocity slice imaging technique [18]. The details of the experimental technique are given in *Methods*. Velocity slice images of H^- at 4.5 eV and 14.5 eV are shown in Fig. 2a and 2b respectively.

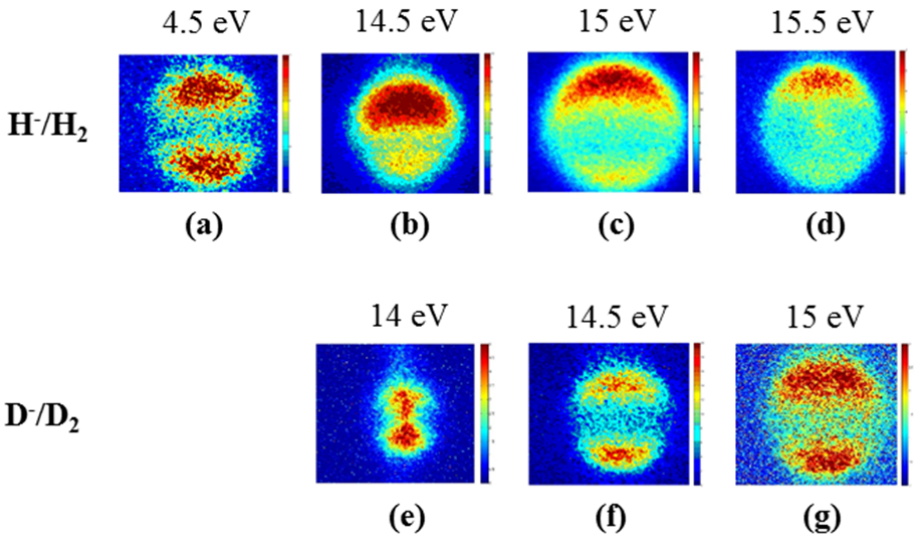

Fig. 2: Velocity slice images of H^- from H_2 at electron energies of (a) 4.5 eV (b) 14.5 eV (c) 15 eV and (d) 15.5 eV and those for D^- from D_2 at electron energies of (e) 14 eV, (f) 14.5 eV and (g) 15 eV. The electron beam direction is from the top to bottom of the figure. Note that while the intensity distribution is symmetric for H^- at 4.5 eV, it is asymmetric at higher energies and that the asymmetry is substantially lower for D^-.

It can be seen that the image at 4.5 eV shows a symmetric distribution in the forward and backward directions and based on Fig. 1b we conclude that the resonant state is of Σ_u^+ symmetry. In contrast to the 4.5 eV image, the 14.5 eV image shows a noticeable forward-backward asymmetry. That the

intensity distribution is parallel to the electron beam implies the contribution from a resonance of Σ_u^+ symmetry. The measurements carried out at higher electron energies show a similar asymmetry in the distribution as can be seen in Fig. 2b to 2d. The results for D_2 in the same energy range are shown in Fig. 2e to 2g. While the images of H^- show a marked asymmetry, the images of D^- from D_2 show much less asymmetry. The slight asymmetry that is present in D^- image appears to change direction with electron energy - at 14 eV the asymmetry is opposite to that seen in H_2, almost symmetrical at 14.5 eV and in the same direction as that in H_2 at 15 eV.

As discussed earlier, due to the inversion symmetry of a homonuclear diatomic molecule, DA through a single NIR will not provide any asymmetry in the angular distribution of the ions. So how might such an observed asymmetry arise? We show below that the asymmetry can be explained in terms of the interference of two dissociating quantum paths if the electron attachment leads to the coherent formation of two NIRs of opposite parity. This takes place by attachment of s-wave (l=0) and p-wave (l=1) of a free electron coherently to form NIRs of Σ_g and Σ_u symmetry respectively. These two NIRs eventually dissociate to the same limit through their respective potential energy curves defining two interfering quantum paths, as shown in Fig. 3. For these two coherently formed NIRs, the angular distribution of the fragment ions is given by

$$f(\theta) = \sigma_{DA_g} + 3\sigma_{DA_u} cos^2\theta + 2cos\varphi cos\theta \sqrt{|\sigma_{DA_g}||\sigma_{DA_u}|} \qquad (1)$$

where σ_{DA_g} and σ_{DA_u} are the DA cross sections for each of the channels contributing and $\sqrt{|\sigma_{DA_g}|}$ and $\sqrt{|\sigma_{DA_u}|}$ indicate the corresponding probability amplitudes of the contributions of the two states to the DA cross section, θ is the angle of ejection of the H^- anion w.r.t. the incoming electron beam and φ is the relative phase between the two channels at the dissociation limit.

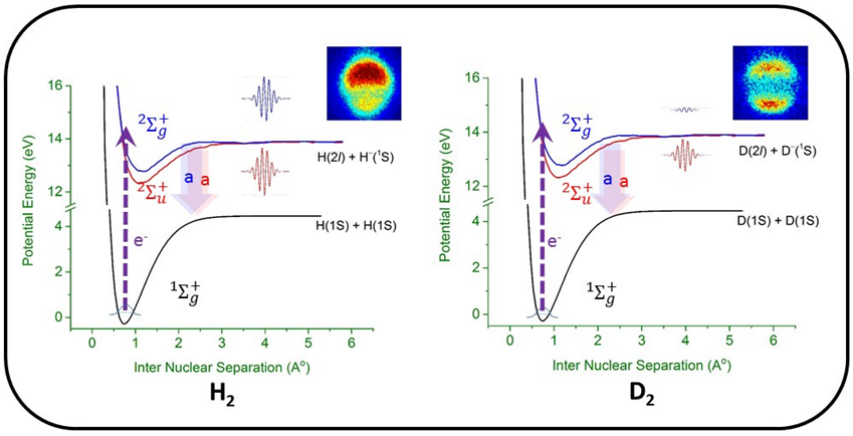

Fig. 3: Schematic of the DA process at 14 eV in H_2 (left) and D_2 (right). The dashed long arrows indicate electron attachment to form the coherent states $^2\Sigma_g^+$ and $^2\Sigma_u^+$. For electron energies above 13.92 eV these states dissociate to form the negative ion (H^-/D^-) and the neutral atom (H/D) in n = 2 state. As the wave packets of these states travel towards the dissociation limits they continuously decay through electron ejection, as shown by the broad faint arrows marked 'a'. For H_2, the wave packets reach the dissociation limit with more or less similar amplitudes, resulting in strong interference and the consequent asymmetry in the momentum distribution as indicated by the velocity slice image. However, for D_2 one of the wave packets has lost most of its amplitude and hence there is a relatively small interference effect, yielding the almost symmetric momentum distribution observed in the image. Please see the text for more details as well as the simulation results given in Fig. 4.

The extent of the asymmetry, which is seen as the contrast in the interference pattern depends on the relative phase between two paths and the relative amplitudes of the wave packets traversing the two paths. Phase differences between these two paths will then occur as the two NIRs evolve along the two distinct potential energy curves. The relative amplitudes of the two paths depend on the capture cross section associated with each NIR and its 'survival probability' against autodetachment which is given by

$$p_i = \exp\left(-\int_{R_c}^{R_\varepsilon} \frac{\Gamma_a(R)}{\hbar v(R)} dR\right) = \exp\left(-\int_{R_c}^{R_\varepsilon} \frac{dt}{\tau(R)}\right) \qquad (2)$$

where $\Gamma_a(R)$ is the width of the anion potential energy curve, $v(R)$ is the speed of separation of the dissociating atoms, R_c is the inter-nuclear separation where the electron capture takes place and R_ε is the effective inter-nuclear separation beyond which the molecular anion is considered to be dissociated. $\tau(R)$ is the corresponding lifetime of the NIR.

Effects due to survival probability are more prominent in the case of heavier isotopes as they have longer dissociation times. As the survival probability of the NIR varies exponentially with the time for dissociation the likelihood of a given resonance surviving against autodetachment in D_2 is considerably smaller compared to that in H_2. This has long been recognised as the basis for the strong isotope effect in DA in molecular hydrogen and its isotopomers [16]. If one of the two coherent NIRs decays much faster compared to the other the contrast of the interference between the two will be weakened. This situation is akin to putting an absorbing material in one arm of an optical interferometer thereby reducing contrast of the interference fringes.

From the momentum images we have derived the forward-backward asymmetry, $\eta = \frac{I_F - I_B}{I_F + I_B}$, at selected energies across the 14 eV resonance where the I_F and I_B are the forward and backward signal strength with respect to the incoming electron beam. These are presented in Table 1. However, it can

be seen that, in the case of H_2, the asymmetry is negative at all energies due to larger backward intensity. The asymmetry in D_2, though small, is in the opposite direction at 14 eV and changes direction as we change the electron energy.

Table 1: Measured forward – backward asymmetry, $\eta = \frac{I_F - I_B}{I_F + I_B}$ for H_2 and D_2 at various electron energies. Please note that negative values of η indicates more intensity in the backward direction and positive values indicate more intensity in the forward direction.

H_2		D_2	
Energy (eV)	$\eta = \frac{I_F - I_B}{I_F + I_B}$	Energy (eV)	$\eta = \frac{I_F - I_B}{I_F + I_B}$
14.5	-0.17	14.0	0.03
15	-0.15	14.5	0.007
15.5	-0.12	15.0	-0.05

In order to model the observed results quantitatively it is necessary to have detailed information on the potential energy curves and lifetimes of the NIRs that are involved. There have been several electron scattering studies on H_2 and D_2 which have provided a wealth of information on their NIRs, as reviewed by Schulz [19]. However, very little information is available for the 14 eV process as compared to that for the 4 eV and 10 eV processes. Transmission as well as scattering experiments had indicated the presence of a $^2\Sigma_g^+$ NIR in the 11eV to 13.5 eV range [20, 21]. The same NIR was identified in the electron scattering experiments at 14 eV with a width of 90 meV [21]. Subsequent DA measurements concluded that this Σ_g^+ NIR is the main contributor to the 14 eV DA process [22] and this has been the accepted wisdom until now [16, 23]. Extensive R-matrix calculations [24] give several NIRs of Σ_g and Σ_u symmetry above 12 eV. However, none of these curves (including their widths) reach the dissociation limit of 13.92 eV in the Franck-Condon region.

One can estimate the amount of forward backward asymmetry for a given electron energy if one knows the potential energy curves for the resonances involved and their widths as a function of inter-nuclear separations. Such an estimate of the asymmetry for two sets of potential energy curves as a function of the lifetime of the *ungerade* state and electron energy is shown in Fig. 4. The asymmetry shows an oscillatory pattern. Please refer the supplementary information for the details of the model. We have used an average lifetime of 8 fs for the $^2\Sigma_g^+$ state based on the reported width of 90 meV at 14 eV [21] and the potential energy curve given by Sharp [25] for the $^2\Sigma_g^+$ state in both the simulations. For the $^2\Sigma_u^+$ state, we have used two different curves. For the results in Fig 4(a) and (c)

the curve that follows the $B^1\Sigma_g^+$ state of the neutral with appropriate energy shift [25] was used. Plots in Fig 4(b) and (d) were obtained by using the potential energy curve that would follow the $C^1\Pi_u$ curve of neutral H_2 [25]. As expected the pattern strongly depends on the potential energy curves as well as lifetimes of the resonance states involved. The overall forward backward asymmetry is seen to oscillate with electron energy. These oscillations are 'faster' if the two dissociating paths are considerably different, as in the case of Fig. 4 (a) and (c) and 'slower' when the two paths are fairly close as in the case of Fig. 4 (b) and (d). The difference between H_2 and D_2 are clearly visible if one compares (a) with (c) and (b) with (d). For a given lifetime of the $^2\Sigma_u^+$ state, the amplitude of the oscillation is smaller in D_2 compared to that in H_2. This is consistent with the qualitative description given earlier and as depicted in Fig. 3. We also note that Fig. (b) and (d) show qualitative agreement with the experimental data (Table 1) and the degree of asymmetry does not change substantially in this case over a range of electron energies as in the case of the measured data for H_2. The directional change of the asymmetry with electron energy in the case of D_2 is also seen. From these qualitative agreements we predict that the two potential energy curves have similar shapes so that the phase difference between the two paths does not change drastically with energy. We wish to point out that curves used in this case are almost empirically chosen and only more accurate potential energy curves along with their lifetimes will allow us to fully understand the details of the coherent dynamics of this DA process.

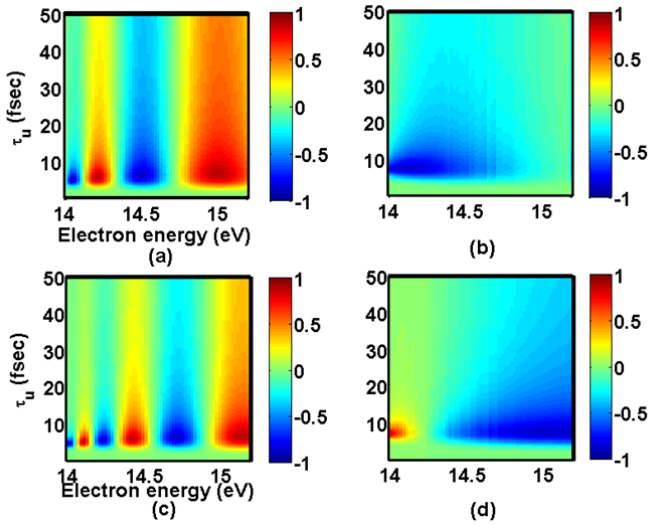

Fig 4: Simulated forward backward asymmetry of the angular distribution for H_2 (top row) and D_2 (bottom row) as a function of electron energy and average lifetime of the $^2\Sigma_u^+$ resonance involved. In all the plots the potential energy (PE) curve for $^2\Sigma_g^+$ state is taken from Sharp [25] and assumed to have an average lifetime of 8 fs. The PE curve for $^2\Sigma_u^+$ state for plots (a) and (c) is assumed to follow the $B^1\Sigma_u^+$ curve with appropriate energy shift and that for plots (b) and (d) it is assumed to follow the $C^1\Pi_u$ from Sharp

194 [25]. The plots (b) and (d) resemble the experimental observation more closely indicating
195 that the approximate potential energy curves used are closer to the real ones (see text).

196 To conclude, coherent excitation of two resonant states of homonuclear diatomic molecule by
197 electron attachment results in symmetry breaking in DA. Such coherence stems from various partial
198 waves of the attaching electron. The resulting quantum paths interfere as they lead to the same
199 dissociation limits. Such a scenario may be observed in particular in electron attachment but may also
200 occur in general in particle scattering as it allows more than one value of angular momentum transfer
201 with comparable strength unlike photoabsorption. It is also interesting to note that the preference of
202 H^- ejection in one direction as against the ejection of excited H atom demonstrates the localization of
203 charge and energy acquired by the molecule in electron attachment. This is also a direct evidence of
204 the role of electron-electron correlations in terms of energy and charge segregation in the dissociation
205 process. The asymmetry in the fragmentation of D_2 is weaker, indicating the reduced strength of the
206 interference in D_2. This is due to the slower dissociation of the resonant states of D_2 resulting in
207 relatively larger depletion of the amplitude of one of the dissociating channels through
208 autodetachment. The situation is similar to two interferometers with different arm lengths and with
209 absorbing medium of differing thickness in the two arms. These results highlight the need, as well as
210 the challenges, to develop a full quantum dynamical calculations for DA to even the simplest system
211 like H_2. Lastly we wish to point out that the formation of coherent states we observe in the DA
212 process may be far more general than has been recognised until now and the signatures of such
213 coherent effects may exist in electron scattering from molecules in general. Moreover, the coherent
214 excitations of anion states also hint at more possibilities of electron induced chemical control.
215
216 References:

217 1. Tichy M. C., Mintert F., and Buchleitner A. Essential entanglement for atomic and molecular
218 physics. *J. Phys. B: At. Mol. Opt. Phys*. **44**, 192001 (37pp) (2011).
219 2. Rice S. A. Interfering for the good of a chemical reaction. *Nature* **409**, 422-426 (2001).
220 3. Rabitz H., de Vivie-Riedle R., Motzkus M., and Kompa K. Whither the Future of Controlling
221 Quantum Phenomena? *Science* **288**, 824-828 (2000).
222 4. Shapiro M. and Brumer P. Coherent control of molecular dynamics. *Rap. Prog. Phys.* **66**,
223 859-942 (2003).
224 5. Sansone G. *et al.* Electron localization following attosecond molecular photoionization.
225 *Nature*, **465**, 763-766 (2010).
226 6. Glover S. C., Savin D. W. and Jappsen A. –K. Cosmological implications of the uncertainty
227 in H^- destruction rate coefficients. *Astrophys. J.* **640**, 553-568 (2006).

7. Kreckel H., Bruhus H., Čižek M., Glover S. C. O., Miller K. A., Urbain X. and Savin D. W. Experimental results for H_2 formation from H^- and H and implications for first star formation. *Science* **329**, 69-71 (2010).
8. Field D. H_2 formation in space: a negative ion route? *Astron. Astrophys.* **362**, 774-779 (2000).
9. Fantz U., Reiter D., Heger B. and Coster D. Hydrogen molecules in the divertor of ASDEX Upgrade. *J. Nucl. Mater.* **290-293**, 367-373 (2001).
10. Taccogna F., Schneider R., Matyash K., Longo S., Capitelli M. and Tskhakaya D. *Contrib. Plasma Phys.* **48**, 147 (2008).
11. O'Malley T. F., Theory of dissociative attachment. *Phys. Rev.* **150**, 14-29 (1966).
12. Van Brunt R. J. and Keiffer L. J., Angular distribution of O^- from dissociative electron attachment to O_2. *Phys. Rev.* A **2**, 1899-1905 (1970).
13. Tronc M., Fiquet-Fayard F., Schermann C. and Hall R I, Differential cross sections and angular distributions of H^- from dissociative electron attachment to H_2 between 3.75 eV and 13 eV. *J. Phys. B: At. Mol. Phys.* **10**, 305-321 (1977).
14. Prabhudesai V. S., Nandi D. and Krishnakumar E., On the presence of the $^4\Sigma_u^-$ resonance in dissociative electron attachment to O_2. *J. Phys. B: At. Mol. Opt. Phys.* **39,** L277–L283 (2006).
15. Gope K., Prabhudesai V. S., Mason N. J., and Krishnakumar E., Probing the resonant states of Cl_2 using velocity slice imaging *J. Phys. B: At. Mol. Opt. Phys*. **49**, 015201 (2016).
16. Krishnakumar E., Denifl S., Cˇadezˇ I., Markelj S. and Mason N. J., Dissociative electron attachment cross sections for H_2 and D_2. *Phys. Rev. Lett.* **106**, 243201 (2011).
17. Cˇadezˇ I., Markelj S., Rupnik Z. and Pelicon P., Processes with neutral hydrogen and deuterium molecules relevant to edge plasma in tokamaks. *J. Phys. Conf. Ser*. **133**, 012029 (2008).
18. Nandi D., Prabhudesai V. S., Krishnakumar E. and Chatterjee A., Velocity slice imaging for dissociative electron attachment. *Rev. Sci. Instrum.* **76**, 053107 (2005).
19. Schulz G. J., Resonances in electron impact on diatomic molecules. *Rev. Mod. Phys*. **45**, 423-487 (1973).
20. Comer J. and Read F. H., Potential curves and symmetries of some resonant states of H_2^-. *J. Phys. B: Atom. Mol. Phys*. **4**, 368-88 (1971).
21. Weingartshofer A., Ehrhardt H., Hermann V. and Linder F., Measurements of absolute cross sections for (e, H_2) collision processes. Formation and decay of H_2^- resonances. *Phys. Rev. A* **2**, 204-304 (1970).
22. Tronc M., Hall R. I., Schermann C. and Taylor H. S. Interference in dissociative attachment cross sections of H_2 around 14 eV. *J. Phys. B: Atom. Mol. Phys*. **12**, L279-L282 (1979).

23. Celiberto R., Janev R. K., Wadehra J. M. and Tennyson J., Dissociative electron attachment to vibrationally excited H_2 molecules involving the $^2\Sigma_g^+$ resonant Rydberg electronic state. *Chem. Phys.* **398**, 206–213 (2012).
24. Stibbe D. T. and Tennyson J., Electron–H_2 scattering resonances as a function of bond Length. *J. Phys. B: At. Mol. Opt. Phys.* **31**, 815–844 (1998).
25. Sharp T. E. Potential-energy curves for molecular hydrogen and its ions. *Atomic Data* **2**, 119-169 (1971).

Methods:

Experimental Apparatus:

We carried out the measurements using velocity slice imaging technique [18]. A schematic of the experimental arrangement is shown in Fig. 5. In this arrangement a pulsed (200 ns pulse duration) electron beam is allowed to interact with an effusive molecular beam produced from a long capillary tube. A low magnetic field (50 Gauss) is used to collimate the electron beam. The product anions are extracted into a velocity mapping time of flight spectrometer mounted at right angles to the electron beam direction using a pulsed electric field after a delay of 200 ns with respect to the electron pulse. The ions are detected using a 2-dimensional position sensitive detector including a Z-stack of three 75 mm diameter microchannel plates and phosphor screen [16]. The image on the phosphor screen is recorded using a CCD camera. Velocity slice imaging can be carried out by pulsing the detector and the phosphor bias corresponding to the arrival of the central slice of the Newton sphere of the relevant ion at the detector - however, due to the low signal levels, data were taken with relatively wide slices.

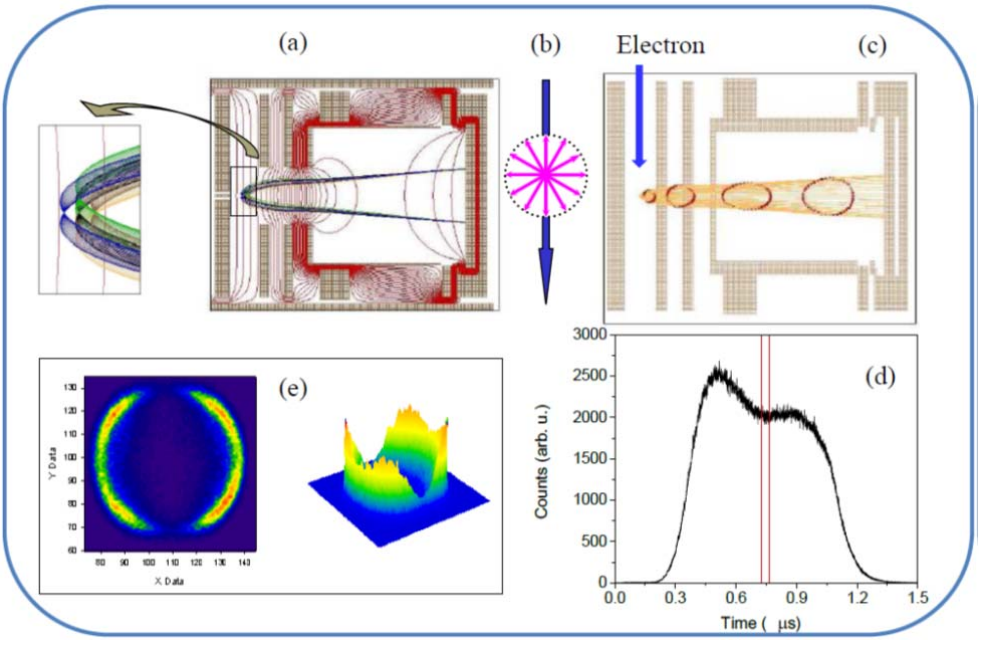

Fig. 5: Schematic of the velocity slice imaging for low energy electron collisions employed in the present measurements. (a) SIMION simulation showing velocity map

imaging. (b) Central slice of the Newton sphere in the plane containing the electron beam (blue arrow) and perpendicular to the time of flight axis. (c) Propagation of the Newton sphere (red circle) in the spectrometer. Note that it is stretched in the longitudinal direction as it moves towards the detector. (d) Time of flight spectrum as the Newton sphere arrives at the detector. The central slice of the sphere is captured (indicated by the region between the two red lines) by having the detector active using a pulsed bias. (e) The resultant velocity slice image.

Model for the forward – backward asymmetry:

With τ_g and τ_u as the average lifetimes of the *gerade* and *ungerade* resonant states involved in DA, t_g and t_u as the dissociation times for the parent anion along the respective potential energy curves for electron attachment with a specified energy and assuming equal capture cross section for both the resonances this asymmetry can be obtained as

$$\eta = \frac{\sqrt{3}\exp[-\left({}^{t_g}/_{2\tau_g} + {}^{t_u}/_{2\tau_u}\right)]}{\exp\left[-({}^{t_g}/_{\tau_g})\right] + \exp[-({}^{t_u}/_{\tau_u})]}\ cos\delta \qquad (3)$$

where δ is the relative phase between the two paths of dissociation for the anion resonant states given by

$$\delta = \frac{1}{\hbar}\int_{R_C}^{\infty}\left[\sqrt{2\mu(E - V_u(R)} - \sqrt{2\mu(E - V_g(R)}\right]dR + \frac{\pi}{2} \qquad (4)$$

Here R_C is the inter-nuclear separation corresponding to the electron capture, μ reduced mass of the dissociating system, E is the electron energy and $V(R)$ is the potential energy corresponding to the given resonant state with respect to the v=0 level of the neutral ground state.